Optical Engineering

SPIEDigitalLibrary.org/oe

Robust particle outline extraction and its application to digital in-line holograms of marine organisms

Nicholas M. Burns
John Watson

SPIE

Robust particle outline extraction and its application to digital in-line holograms of marine organisms

Nicholas M. Burns* **and John Watson**
University of Aberdeen, School of Engineering, Aberdeen AB24 3UE, Scotland

Abstract. Digital holography offers a method of high-resolution imaging of microscopic particles and organisms in their natural environment. Automated image extraction and data processing are essential for rapid interrogation and analysis of the vast amounts of information contained in a typical hologram. In this work, we describe a robust-automated particle focusing approach, which we have developed to extract outlines of all particles contained within the sampling volume of each hologram constituting a "holovideo." The output data consists of ordered point-lists delineating polygons that match particle outlines and facilitate further processing such as extraction of focused images from the holograms themselves. The algorithm developed allows the reduction of, typically, a 2-GB holovideo to tens of megabytes, thereby greatly reducing analysis time by allowing rapid scanning of the contoured images without manual focusing. The algorithm has been demonstrated on synthetic and laboratory holograms and applied to holographic videos recorded in the North Sea. The algorithm output also lends itself to further automated analysis techniques like particle tracking or automated recognition. © *2014 Society of Photo-Optical Instrumentation Engineers (SPIE)* [DOI: 10.1117/1.OE.53.11.112212]

Keywords: digital holography; submersible holography; autofocusing algorithms; image processing.

Paper 140188SS received Jan. 31, 2014; revised manuscript received Apr. 10, 2014; accepted for publication Apr. 29, 2014; published online May 28, 2014.

1 Introduction

Since the demonstration of direct hologram recording on an image sensor array followed by numerical reconstruction,[1] digital holography (DH) has grown in popularity for high-resolution imaging of microscopic particles in air and underwater. Following Owen and Zozulya's seminal paper,[2] several research groups have developed submersible digital "holocameras" to monitor plankton and other marine organisms.[3–5] A key difficulty in DH of small particles, however, is not in the recording but in the extraction, analysis, and evaluation of the vast amounts of data contained in a hologram or holographic video (holovideo). Although manual scanning is possible, automated focusing, particle tracking, and data extraction are essential in any practical situation. Several methods of hologram autofocusing have been reported. Some of the more successful include selfentropy,[6] l-1 norms,[7] Fresnelet-sparsity,[8] and amplitude analysis.[9] Our approach is based on contour generation followed by gradient measurement around the particle edges, relying upon spatial domain data extracted from reconstructions performed at regular intervals through the hologram volume.

2 Hologram Recording and Reconstruction

In DH, the holographic interference field is directly recorded onto an electronic imaging sensor, and a full-volume image is subsequently reconstructed by computer simulation of the propagation of the field through space. Subsea holocameras usually employ in-line recording: i.e., the illuminating laser beam passes through the sample volume to the sensor; image planes are reconstructed at any distance from the hologram and at any time frame. Our digital holocamera (described in detail by Sun et al.[3,10]), "eHoloCam" records in-line holograms on a complementary metal oxide semiconductor image sensor (IBIS 4-6600; 10.5 mm by 7.72 mm; 3000 by 2208, 3.5-μm-square pixels; 25-Hz maximum frame rate) using a pulsed, frequency-doubled Nd-YAG laser (532 nm; 4-ns pulses; up to 25-Hz repetition rate). Collimated beam illumination over a path length of 450 mm gives a sampling volume of about 37×10^3 mm^3.

The reconstruction algorithms employed are usually based on the Fresnel–Kirchhoff integral and implemented using the Fresnel approximation or convolution to aid efficient computation.[11] We use the angular-spectrum approach (a variation on convolution),[12] which decomposes the hologram into its constituent spatial frequencies using a Fourier transform (FT) before multiplying with a propagation matrix to modify the phase of each component of the image spectrum according to distance.[13,14] A final, inverse-FT recombines the frequency components back into the spatial domain to generate a reconstructed hologram image at the required distance from the hologram plane. This approach provides a number of benefits for subsea DH. First, there is no pixel scaling between the hologram and its reconstruction, and particles are replayed at their original size regardless of distance from the hologram. Second, after transformation to its spectrum, unwanted frequencies may be eliminated before it is reconstructed.[15] Finally, since there is no minimum reconstruction distance imposed before the algorithm breaks down, it allows the entire hologram volume to be scanned.[16]

This focusing algorithm was developed for field holograms recorded in the North Sea with "eHoloCam."[3] However, it has more general applicability. It has been evaluated in three different cases: (1) a synthetic (simulated) reference hologram [Fig. 1(a)] created in MATLAB® of

*Address all correspondence to: Nicholas M. Burns, E-mail: n.m.burns@abdn.ac.uk

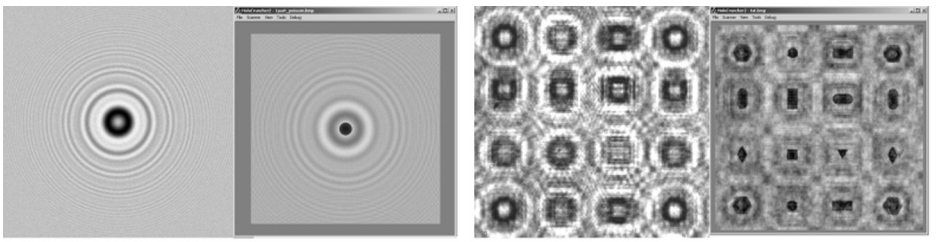

(a) (b)

Fig. 1 (a) Hologram of a 300-mm sphere synthesized on a 4.65-mm square pixel pitch, 632.8-nm wavelength (left) and its reconstruction (right); (b) laboratory hologram of objects with a 200-mm edge on a 1-mm grid, recorded on a 3.5-mm square pixel pitch at 632.8-nm (left) and its reconstruction (right).

a sphere of 300-μm diameter on a 4.65-μm-square pixel pitch at 632.8-nm wavelength; (2) a laboratory reference hologram [Fig. 1(b)] of a photolithographically produced target composed of a series of shapes each with a 200-μm edge, on a 1-mm grid (the corresponding hologram was recorded on a 3.5-μm-square pixel pitch at 632.8 nm); and (3) a series of field holograms of plankton recorded in the North Sea (Sec. 3).

3 Focusing Techniques and the Contour Gradient Algorithm

A first step in interpretation of "holovideos" involves localizing every particle within a frame (in spatial and time dimensions) and distilling particle shape and positional information from gigabytes of hologram data. For each video frame, the hologram is focused in incremental steps and an image of each slice parallel to the sensor plane is reconstructed. This is equivalent to discretized simulation of the wave-field projected into real image space by an analogue hologram when reconstructed by an optical beam. When a reconstruction plane coincides with a particle it will appear in-focus, characterized by a maximization of image gradients at the particle edges. This facilitates application-specific processing; subsequent image recognition, particle tracking, counting, and sizing can be added at a later date.

A large number of possible focus metrics are used for classical imaging, which depend variously on image gradient, variance, correlation, histograms, and frequency domain analysis.[17] All rely on the premise that focused images have higher information content than blurred images due to the existence of larger gradients and higher variance across them. This leads to a greater deviation between maxima and minima in the brightness histogram and the local maximization of power in higher frequency components, when the image is transformed to the frequency domain.

Holographic images pose certain problems that make focus detection somewhat difficult to implement. Most problematic is the ever-present speckle which manifests itself as high-frequency noise across the image area, and while it can be reduced with local averaging, this tends to sacrifice edge sharpness and reduce its effectiveness. Conversely, applying sharpness metrics to images containing speckle can result in false maxima if there is insufficient noise immunity. Since particles in the hologram are generally much smaller than the reconstructed area, it is difficult to reliably discriminate between focused and unfocused planes above background speckle noise. This can be partially overcome by applying the metric over restricted regions surrounding particle shadows. Since our holograms often contain many particles, it is vital to reduce the measurement area to regions of interest (ROIs) enclosing each particle in the $X-Y$ plane and to maximize the focus measure over each region along the Z-axis. Another disruptive effect is that images do not defocus in a uniform manner as in conventional photography. High-frequency fringes begin to form around the particles as the diffraction orders move out-of-phase with respect to one another. In some cases, these fringes can generate edges that appear stronger to sharpness functions than those at the focal plane, resulting in false maxima. In a defocused hologram, all frequencies associated with a particle will be present over a comparatively wide focal range. Frequency domain focusing methods based on high-frequency maximization are not easily applied in DH, even in small regions surrounding particles.

In an earlier work,[18] the "Tenengrad" approach was shown to have some inherent weaknesses for holography of subsea organisms. This led us to investigate a new approach, dubbed "contour gradient," which was devised to overcome many of these difficulties. Before describing the contour generation, we summarize first our results with Tenengrad. Our implementation of Tenengrad differs slightly from the formal approach by inclusion of a normalization factor related to the size of the region to which it is applied. This is necessary to compensate for variations in automatically generated ROI dimensions within a single ROI group, caused by variations in particle shadow size along the Z axis of the hologram volume. We also often introduce a threshold which prohibits the addition of the absolute pixel gradient to the sum unless the gradient is greater than our chosen threshold. Although this threshold is usually unnecessary in classical imaging, it is invaluable in increasing the noise immunity of the algorithm when applied to holographic images with substantial speckle noise. The threshold must be kept low enough, though, so that particle edges continue to contribute to the sum. Selection of a suitable threshold is performed experimentally using a sample hologram from the recording system. We begin with a zero threshold and increase in increments of 10 to maximize the peak strength seen in the metric response for a single scan. Once a suitable threshold is identified, it will generally obtain similar results for subsequent holograms recorded by the same system due to the similar speckle magnitude in each hologram. The threshold effectively sets an upper limit on the speckle amplitude which

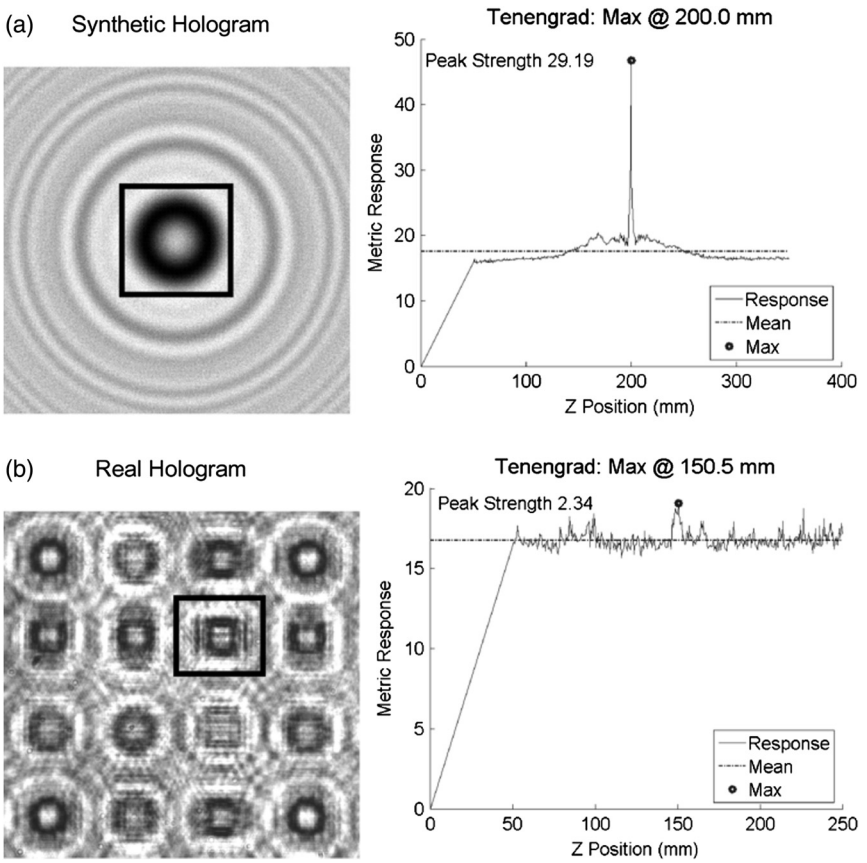

Fig. 2 Tenengrad applied to (a) a synthetic hologram and (b) a real laboratory hologram. The region to which Tenengrad was applied is marked by the black rectangles.

can be rejected, thus holograms containing minimal speckle such as the synthetic hologram of Fig. 2 will continue to generate a peak without further tuning of the threshold.

The major weakness of Tenengrad in DH lies in its indiscriminate application to all pixels within a ROI. Speckle noise can contribute substantially to the Tenengrad measurement, resulting in a high background noise in the response. Figure 2 shows Tenengrad applied to both synthetic and laboratory holograms shown in Fig. 1. The synthetic hologram produces a very pronounced, narrow peak of 29.19 arbitrary units above the mean background, and correctly identifies the focal plane. The synthetic hologram serves as a reference for comparison with the field holograms and is a good indicator of the maximum achievable response. This performance is not matched in the laboratory hologram, for which the correct plane is identified, but the peak of only 2.34 units above the mean response increases the likelihood of false focus detection.

A further weakness exists when using $X-Y$ aligned ROIs. ROI generation performs a merging stage, after the initial processing of a plane, in order to reduce the number of ROIs generated and to recombine particles that break up into two or more ROIs. This step aids in tracking individual particle shadows in the hologram volume, but introduces a trade-off between maximum particle density and reliability of particle tracking. Particular problems that may arise are illustrated in the diagrammatic representations of Fig. 3, which show geometries that can result in two or more ROIs overlapping and merging into a single ROI.

Our improved focus metric is a variation on Tenengrad and restricts the number of pixels that contribute to the gradient measurement to those in the vicinity of particle edges. It identifies possible particle edges using a contouring algorithm applied to reconstructed planes, and gradients are summed along those edges only [Eq. (1)].

$$C\text{grad} = \frac{1}{N}\sum_{n=0}^{N}\sqrt{S^2_{x[Pn(x),Pn(y)]} + S^2_{y[Pn(x),Pn(y)]}}, \tag{1}$$

$$\text{Mask}_x = \begin{bmatrix} -1 & 0 & 1 \\ -2 & 0 & 2 \\ -1 & 0 & 1 \end{bmatrix}, \quad \text{Mask}_y = \begin{bmatrix} -1 & -2 & -1 \\ 0 & 0 & 0 \\ 1 & 2 & 1 \end{bmatrix},$$

$$S_{x(x,y)} = \sum_{i=-1}^{1}\sum_{j=-1}^{1}\text{Mask}_{x(i+1,j+1)}\text{Im}_{(i+x,j+y)}, \tag{2}$$

$$S_{y(x,y)} = \sum_{i=-1}^{1}\sum_{j=-1}^{1}\text{Mask}_{y(i+1,j+1)}\text{Im}_{(i+x,j+y)}. \tag{3}$$

In the above, N represents the number of points in a contour, and P_n represents a point at index n. The Sobel operators [Eqs. (2) and (3)] are applied as for Tenengrad; however, the positions at which they are applied are guided

by the (x, y) coordinates of the points comprising the contour. Again, we introduce a normalizing factor, dividing the total sum by the number of points measured to provide length-invariance to the metric. This is applied to all contours within an image, giving each separate contour a unique gradient measure. Focused planes are identified by grouping similar-shaped contours through Z and finding the contour in each group that produces the maximum response.

The major benefits of this approach are twofold. First, the reduction of the number of pixels decreases the impact of speckle noise and increases the amplitude of the focused response above background. Second, contours provide a more accurate representation of particle position and can support higher particle densities and geometries that are problematic in the ROI generation. The failure examples shown in Fig. 3 are readily handled when particles are located by contours. We have also successfully applied this technique to holograms of spherical particles to provide an initial estimate for the positioning of point-sources in a least-squares minimization algorithm capable of identifying particle focal planes on the order of micrometers.[19]

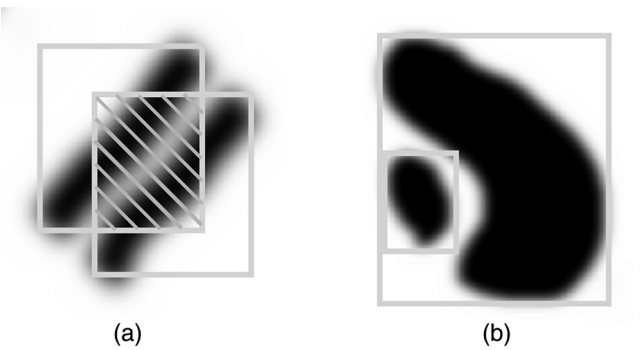

Fig. 3 Diagrams of geometries that can produce region of interest (ROI) generation failure. (a) Substantial overlap (indicated by hatching) causes ROIs to merge. (b) Total overlap causes smaller ROI to be absorbed in larger ROI.

To compare Tenengrad independently from the particle tracking performed by the ROI generation or contour matching, we measure the contour gradient within the same manually selected ROI. Contours are generated only within this region, and the contour gradient is obtained at each Z plane. Figure 4 illustrates the contour gradient response for the same holograms as in Fig. 2. The peak strength of the synthetic hologram has increased by one-third (to 41.60 units above mean background); and for the laboratory hologram it has nearly doubled (to 4.03 units above mean background). This indicates more robust detection of the focal plane and is replicated in other opaque particle holograms that we have analyzed. We also note a variation in the identified focal plane for the laboratory hologram between Tenengrad (150.5 mm) and the contour gradient (149.0 mm). Figure 5 illustrates an object selected from the reference hologram and brought to a focus using both algorithms: the images are qualitatively similar, although the top edge appears marginally sharper for the contour gradient. Figure 6 illustrates a copepod from the North Sea plankton holograms: the

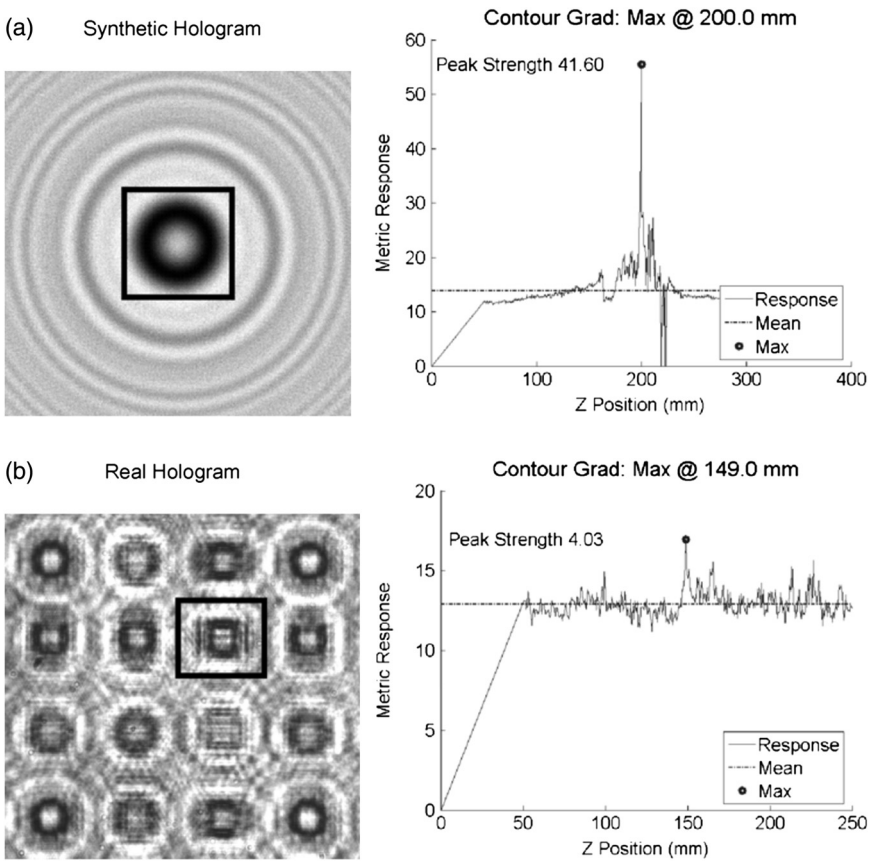

Fig. 4 Contour gradient applied to (a) a synthetic hologram and (b) a real laboratory hologram. The region to which the contour gradient was applied is marked by the black rectangles.

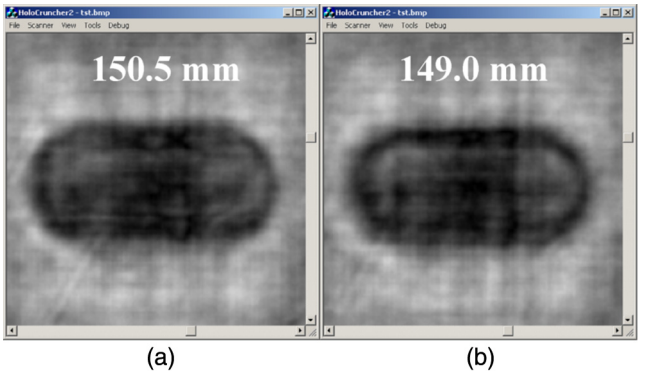

Fig. 5 Reconstructions of target particle in the laboratory hologram at planes identified by (a) Tenengrad, and (b) contour gradient algorithm.

Tenengrad peak is 1.96 above the mean level whereas the contour gradient peak is 11.72 above the mean. The detected foci are at 280.5 and 282.0 mm, respectively.

Since the contour gradient localizes particles with closely fitted polygons, the particle density that can be handled approaches the theoretical maximum that can be recorded with in-line holograms while still maintaining acceptable signal-to-noise ratios (SNRs). Meng[20] developed an expression to quantify the SNR for in-line holograms recorded on photographic film and application of this indicates that about 30 particles per centimeter cubed of 200-μm diameter over a 450-mm path length could be successfully recorded on film. We have not verified this experimentally for digital holograms, but observation indicates that this predicted maximum may be optimistic for nonspherical particles.

Any algorithms capable of generating (preferably ordered) point lists based on a threshold value across a two-dimensional sampled surface are suitable for use as the contour generation algorithm. Benefits can be gained, however, in reduced processing time and code complexity by developing a tailored algorithm that applies the Sobel operators while it generates the contours. After contour generation, a similarity test is implemented to assign identification (ID) numbers to each contour. The initial plane has its contours assigned arbitrary ID numbers as there are no previous planes to refer to; however, subsequent planes require each new contour to be compared with those on the previous plane, with ID numbers carried forward onto sufficiently similar contours. This labels contour groups that persist through several reconstructed Z planes and can be assumed to outline the same particle at its various levels of focus.

The final extraction of outlines involves processing each ID group in turn and identifying the plane on which the maximum contour gradient exists for each group. These gradient maxima should indicate the focal planes of particles, while the contours give the particle outline. This is particularly beneficial if only particle tracking is of interest, since there is no need to extract particle images. The contours can also be readily used to compute particle cross-sections and centroids based on well-known geometric algorithms, provided they have been generated as ordered point lists. The resulting focused contours are stored in an output file which can be manually inspected to find particles of interest

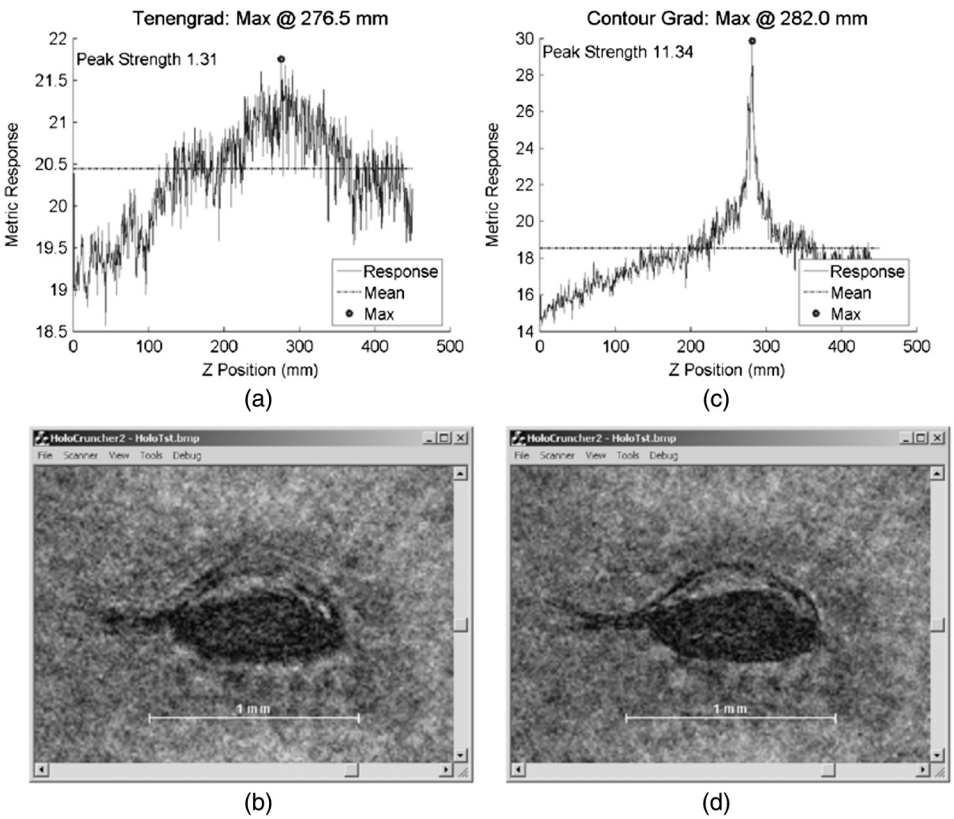

Fig. 6 Response of metric for a sample particle (a) at plane identified by Tenengrad (b) and response (c) for particle at plane identified by contour gradient (d).

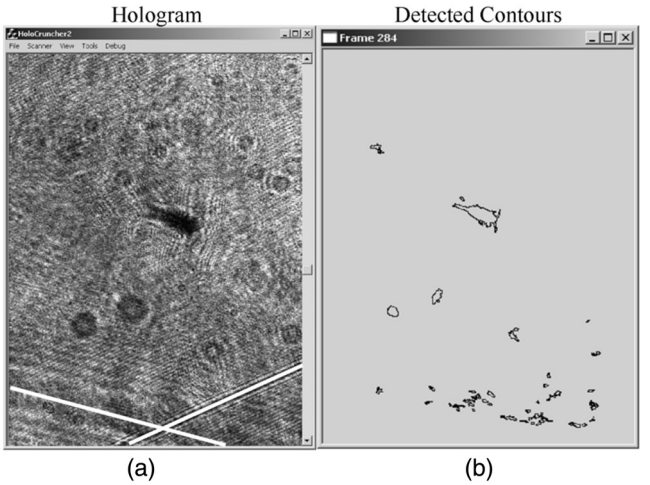

Fig. 7 (a) Sample plankton hologram frame (fiducial wire positions shown in white). (b) Contours generated in output file by contour gradient scan.

using their outline only. Images of particles can then be reconstructed with ease.

4 Contour Gradient Scan Results for Subsea Holograms

The full contour gradient algorithm has been used to analyze a number of holographic videos recorded in the North Sea. Processing involves automated scanning of each frame and generating an output file which can quickly be manually inspected to find particles of interest or submitted to further automated analysis (which we have not yet implemented). This process typically reduces a 2-GB holovideo, of approximately 1000 frames, to tens of megabytes, thereby greatly reducing the time required to identify particles of interest by allowing manual scanning without the need to manually focus holograms. Figure 7 shows a hologram frame recorded on a 10.5-μm-pixel pitch, and the associated contour output generated for the frame. In-house software facilitates manual inspection by allowing the user to click on a contour loaded from the scan output file in order to recover a reconstructed image of the particle from the original holovideo. Figure 8 illustrates three such particles found in a single frame.

Many of the smaller contours in Fig. 8 are erroneously generated; however, larger particles (above 250 μm—around 25 pixels) are reliably detected. "False alarms" are often seen in regions containing features that are never brought fully into focus and are the result of localized darkening of reconstructed planes due to shadows of these unwanted artifacts. In the plankton holograms, fiducial wires were placed on both input and output windows: these are seen at the bottom of the frames and although outside the scanned volume, their influence extends through the entire volume. Increasing the minimum contour length decreases the likelihood of false contour generation by filtering out smaller objects. There is a trade-off, however, as some contours localize particles as small as 100 μm. For smaller particles, it is advisable to increase the resolution of the image sensor for more reliable detection.

Certain particles still cause difficulties in focusing due to the presence of transparent regions or distribution of focus along the Z-axis of the hologram (e.g., some plankton have tails that may lie in a different Z-plane to their heads). Figure 9 illustrates particular failures which are seen in the datasets from the North Sea holograms. Figure 9(a) shows the separation of contours for a particle with an opaque head and partially transparent tail. This is difficult to overcome, as the tail forms a complicated structure which produces many separate, small contours due to the refraction of the recording beam through the tail. This particular example is also difficult to focus manually for the same reason. Figure 9(b) illustrates a similar failure in which the transparency of the particle has produced incorrect results. When manually focused, only a fine outline is formed around the transparent body of the particle. Features such as these often produce strong diffraction fringes some distance from the ideal focal plane, and result in misinterpretation by the contour gradient algorithm.

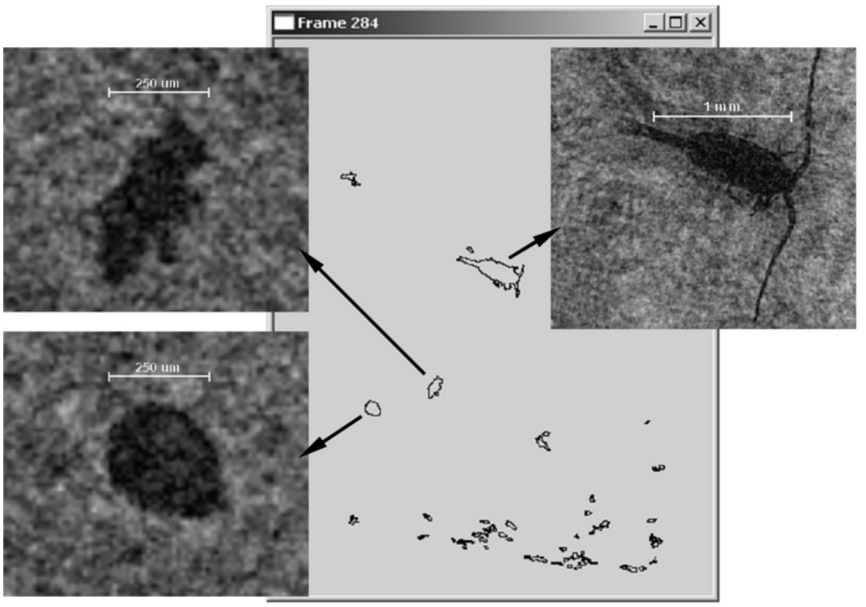

Fig. 8 Images of reconstructed particles using contours to locate them in the holovideo.

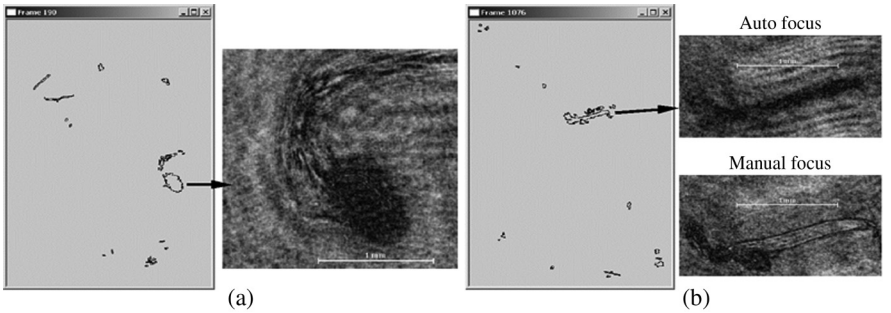

Fig. 9 (a) Illustration of breakup of particles with transparent regions. (b) Failure to identify correct focal plane for a particle with transparent regions.

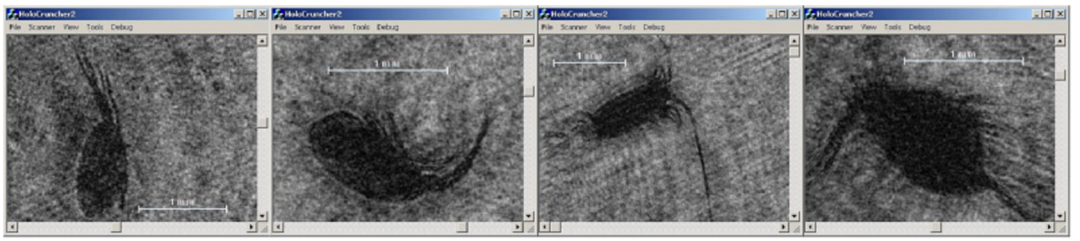

Fig. 10 A collection of copepod images obtained from a single holovideo using the contour gradient scan.

Figure 10 shows a number of Calanoid copepods that have been detected in a single holovideo by the contour gradient scan and found by manual inspection of the contours. The contour gradient algorithm has shown excellent performance in focusing on this type of organism, and it is possible to manually scan the generated contour file to quickly locate their distinctive outline.

For a more quantitative assessment of its performance, we scanned a series of holovideos, using the contour gradient method, which had previously been manually scanned for copepods and reported by Sun et al.[3] (holovideos VD6 and VD7 of that article). A summary of the results is given in Table 1. In the original manual scans, images were not taken of all the copepods detected, therefore, we are unable to say if all the same organisms were observed in each case and can only compare numbers. For VD6, 13 definite observations of copepods were made compared with 9 with the all-manual method. In VD7, 29 positive identifications were made using the contour gradient approach compared with 34 in the original manual scan. At least two copepods for which images were recorded manually were not picked up by the automatic method: one was an organism at the edge of a frame, and in the other, the resolution of the copepod image was too low to be easily detected by the contour gradient. Video VD6 was recorded at a pixel pitch of 7 μm, whereas VD7 was at the lower resolution of 10.5-μm pixel pitch which may account for the missed detections. Although it can take up to two months to scan an entire video (depending on the number of frames) manual scanning of the contour frames takes only a few minutes to detect the most likely contours. Further analysis of the entire set of holovideos is being undertaken and will be reported in another article.

Table 1 Comparison of manual and semiautomatic scanning of subsea holovideos.

Video	Video resolution	No. of frames	Towed depth range (m)	No. of copepods (manual)	No. of copepods (auto)
VD6	Medium (7.5-μm pixel)	1190	99 to 104	9	13
VD7	Low (10.5-μm pixel)	2627	95 to 103	34	29

5 Conclusions

Although digital in-line holography is ideally suited for capturing microscopic particles and their distribution, the processing stage often causes difficulties due to the vast amount of data in a hologram. When applying Tenengrad as a focus metric, it is difficult to implement a reliable ROI generation scheme that does not merge closely spaced particles. Furthermore, the algorithm itself can be disturbed by strong diffraction fringes in the vicinity of particles, or by excessive speckle noise. To remove these weaknesses we implemented a new particle localization scheme based on contours instead of rectangular ROIs, allowing more reliable decoupling of closely spaced particles. The focus metric was then reduced from measuring the gradients of all pixels within a ROI to measuring gradients only along the contours, thereby considering only those areas of reconstructions in which edges would be expected to be present. We have shown that applying the gradient measure to particle edges in this manner produces substantially stronger responses in the focus metric.

We consider the contour gradient algorithm to be sufficiently well-developed to be applied to the analysis of

holograms of plankton and other marine organisms and particles. Its application shows reliable focus detection for larger, opaque particles such as copepods. The output from the contour gradient algorithm allows rapid manual inspection, since many species can be recognized from their outlines with little practice. Comparison with previous manual scanning of holovideos recorded in the North Sea showed that the contour gradient approach detected similar numbers of organisms; however, the algorithm did fail to focus some particles near the frame edges. Transparent particles have also been shown to cause difficulties with the scanning process. Further work may improve on the "false" detections of particles in the size range of fewer than 25-pixels diameter, however, speckle will always cause problems at this size; a more reliable solution for imaging smaller particles is to increase the image sensor resolution. It is our intention now to develop further automated analysis methods to process the contour data, such as image classification and time-domain particle tracking.

Acknowledgments

The authors wish to thank Mr. E. Kamau, BIAS, Germany, for the use of the synthetic hologram in Fig. 1(a) and Prof. V. Dyomin, Tomsk State University, Russia, for the use of the laboratory reference hologram in Fig. 1(b). We also wish to thank Dr. Hongyue Sun for the laborious manual scans of the holovideos.

References

1. U. Schnars and W. Jüptner, *Digital Holography*, Springer, Berlin, Heidelberg (2005).
2. R. B. Owen and A. A. Zozulya, "In-line digital holographic sensor for monitoring and characterizing marine particles," *Opt. Eng.* **39**(8), 2187–2197 (2000).
3. H. Y. Sun et al., "In situ electronic holographic camera for studies of plankton," *IEEE J. Ocean Eng.* **32**(2), 373–382 (2007).
4. S. K. Jericho et al., "Submersible digital in-line holographic microscope," *Rev. Sci. Instrum.* **77**, 043706 (2006).
5. J. Sheng, E. Malkiel, and J. Katz, "Digital holographic microscope for measuring three-dimensional particle distributions and motions," *Appl. Opt.* **45**(16), 3893–3901 (2006).
6. R. A. King, "The use of self-entropy as a focus measure in digital holography," *Pattern Recognit. Lett.* **9**(1), 19–25 (1989).
7. W. Li et al., "Focus detection from digital in-line holograms based on spectral l-1 norms," *J. Opt. Soc. Am. A* **24**, 3054–3062 (2007).
8. M. Liebling and M. Unser, "Autofocus for digital Fresnel holograms by use of a Fresnelet-sparsity criterion," *J. Opt. Soc. Am. A* **21**(12), 2424–2430 (2004).
9. F. Dubois et al., "Focus plane detection criteria in digital holography microscopy by amplitude analysis," *Opt. Express* **14**, 5895–5908 (2006).
10. H. Sun et al., "Underwater digital holography for studies of marine plankton," *Philos. Trans. R. Soc. A* **366**(1871), 1789–1806 (2008).
11. D. C. Champeney, *Fourier Transforms and Their Physical Interpretation*, Academic Press, London (1973).
12. H. Dong et al., "Algorithms and applications for electronically recorded holography," *Proc. SPIE* **5477**, 354–365 (2004).
13. E. Cuche, F. Bevilacqua, and C. Depeursinge, "Digital holography for quantitative phase-contrast imaging," *Opt. Lett.* **24**(5), 291–293 (1999).
14. C. J. Mann, L. Yu, and M. K. Kim, "Movies of cellular and sub-cellular motion by digital holographic microscopy," *Biomed. Eng. Online* **5**, 21 (2006).
15. T. Colomb et al., "Total aberrations compensation in digital holographic microscopy with a reference conjugated hologram," *Optics Express* **14**(10), 4300–4306 (2006).
16. E. Malkiel, J. N. Abras, and J. Katz, "Automated scanning and measurements of particle distribution within a holographic reconstructed volume," *Meas. Sci. Technol.* **15**(4), 601–612 (2004).
17. A. Santos et al., "Evaluation of autofocus functions in molecular cytogenetic analysis," *J. Microsc.* **188**(3), 264–272 (1997).
18. N. M. Burns and J. Watson, "A study of focus metrics and their application to automated focusing of in-line transmission holograms," *Imaging Sci. J.* **59**(2), 90–99 (2011).
19. E. Kamau et al., "Least-squares based inverse reconstruction of in-line digital holograms," *J. Opt.* **15** 075716 (2013).
20. H. Meng, "Intrinsic speckle noise in in-line particle holography," *J. Opt. Soc. Am.* **10**(9), 2046–2058 (1993).

Nicholas M. Burns graduated in electronic and computer engineering in 2005 and obtained his PhD in digital holography from the University of Aberdeen in 2011. He has spent several years at the University of Aberdeen as a researcher in optical engineering. His work encompasses digital holographic recording and processing techniques and has expanded into optical instrumentation for oil and gas. His research interests lie in underwater holography, optical sensors, and computational methods to analyze holograms.

John Watson graduated in physics in 1973 and obtained his PhD in laser microspectral analysis from St. Andrews University in 1978. After 5 years with the UKAEA, Scotland, he returned to the academic world. He holds the Chair of Electrical and Optical Engineering at Aberdeen University. His research interests lie in underwater holography, subsea laser welding, and laser microspectral analysis. He is a fellow of IET, IoP and a senior member of IEEE.